J. Fluid Mech. (1984), *vol.* 145, *pp.* 179–199
Printed in Great Britain

The rate of coagulation of a dilute polydisperse system of sedimenting spheres

By ROBERT H. DAVIS
Department of Chemical Engineering, University of Colorado, Boulder, Colorado 80309

(Received 25 July 1983 and in revised form 1 February 1984)

We consider a dilute dispersion containing small rigid particles in a Newtonian fluid. These spherical particles are of different size and density, and they settle relative to one another under the action of gravity. When the particles become close, they exert an attractive van der Waals force on each other, and doublets are formed when two particles come into contact as a result of this force. The rate at which doublets are formed is calculated using a trajectory analysis to follow the relative motion of pairs of particles.

We restrict our attention to dispersions where the Péclet number is large (negligible Brownian motion) and where the Reynolds number is small (negligible fluid inertia). However, the effects of the inertia of the particles on their trajectories are included, and these are measured by the Stokes number. A key dimensionless parameter is identified, denoted by Q_{ij}, which provides a measure of the relative importance of gravity and the van der Waals force. An asymptotic solution to the trajectory equations is presented for large values of this parameter in the case of zero Stokes number. This asymptotic solution is then complemented by numerical computations of the particle trajectories. Application to typical hydrosol and aerosol dispersions is presented, and, in particular, a comparison is made between the effects of van der Waals forces and Maxwell slip in promoting collisions between aerosol particles.

1. Introduction

In this paper we shall consider the rate of caogulation of small particles in a dilute, statistically homogeneous dispersion. The particles are of different size and density and hence are in relative motion due to their different settling speeds under gravity. When the particles are close, they exert an attractive van der Waals force on each other, and doublets are formed when two particles come into contact as a result of this force. The rate at which the dispersion becomes coagulated is in large part determined by the rate of doublet formation, and it is this quantity that we seek to determine. Furthermore, we shall assume that the particles are sufficiently large so that Brownian motion is negligible (large Péclet number), but not so large that the inertia of the surrounding fluid is important (small Reynolds number). For a typical hydrosol or aerosol dispersion, these restrictions require that the particle radii lie between about 2 μm and 30 μm. In aerosols the density of the particles is much greater than that of the surrounding air, and often the inertia of the particles significantly influences their motion (large Stokes number) even when the inertia of the surrounding air is negligible. The effects of particle inertia will be included in our analysis.

The first attempts to estimate the rate of coagulation of a dispersion were made by Smoluchowski (1917). In his simple model, the spherical particles were assumed

to move independently, i.e. without any hydrodynamic interaction or interparticle force other than a sticking force on contact. When hydrodynamic interactions are included, the particles are caused to flow around each other, and, since the resistance to relative normal motion increases as the gap between the particles decreases, actual contact does not occur unless an attractive interparticle force is present.

In a study related to the present one, Zeichner & Schowalter (1977) included the effects of hydrodynamic interaction and interparticle force, and computed the rate of coagulation of a dispersion of equal spheres subject to simple laminar shearing and to uniaxial extensional flow. As with the present work, attractive van der Waals forces cause two particles to come into contact once they pass sufficiently close to each other. These authors used a trajectory analysis to follow the relative motion of the two spheres, and the locus of trajectories that begins with the spheres far apart and terminates with the spheres coming into contact was found. From this trajectory analysis, the collision rate was determined and, provided that the flow is sufficiently strong, was found to be proportional to the shear rate raised to the 0.77 power for shear flow, and to the 0.86 power for extensional flow, instead of to the first power as in Smoluchowski's result. Curtis & Hocking (1970) also performed a similar calculation for shear flow, and in addition report the results of experiments designed to show the ability of van der Waals forces to cause collisions in shear flows. In a more recent work, Adler (1981) has considered the coagulation of unequal spheres in simple shear flow. He found that the collision efficiency (defined as the ratio of the actual collision rate to that when the two particles are assumed to move independently) becomes very small as the ratio of the radius of the smaller sphere to that of the larger sphere is decreased. This result is primarily due to the fact that then the small sphere closely follows the fluid streamlines that flow around the larger sphere.

In another related work, Hocking & Jonas (1970) included the effects of particle inertia and computed the collision efficiency of small water droplets in air falling under gravity – a problem of particular relevance to the rate of formation of larger drops in a rain-bearing cloud. These authors did not include an interparticle force, and hence actual contact was not possible. Instead, collisions were assumed to occur once the gap between the particles had become some small fraction ϵ of the larger drop radius. Later, Hocking (1973), Jonas (1972), and Davis (1972) modified the Stokes equations for the hydrodynamic interaction by allowing for Maxwell slip to occur at the drop surfaces when the distance between the surfaces became comparable with the mean free path of the surrounding air molecules. This allowed for actual collisions to take place and removed the need for the arbitrary parameter ϵ.

In this paper, a trajectory analysis will be used to compute the rate of doublet formation from a dispersion of spheres of different size and density settling under gravity. In §2 the trajectory equations will be formulated for the case of negligible particle inertia, and expressions will be given for the assumed interparticle force potential and for the collision rate. In §3 we shall solve these equations asymptotically for large values of the parameter Q_{ij} (defined in §2). In §4 we shall present trajectory equations for the motion of two spheres when particle inertia is important. The results of numerical computations for several values of the various parameters will then be presented and discussed. Finally, in §5 the computed collision efficiency as a function of particle size for typical hydrosol and aerosol dispersions will be given. In particular, the application to the coalescence of small droplets in clouds will be discussed, and we shall compare the collision efficiency resulting from van der Waals forces, from Maxwell slip, and from these two effects combined.

2. Trajectory equations for negligible inertia

The particles are assumed to be rigid spheres and are suspended in a Newtonian fluid of density ρ and viscosity μ. The radius, density, number density, velocity, and velocity in isolation of each particle of species i are denoted respectively by a_i, ρ_i, n_i, $\boldsymbol{U}_i$ and $\boldsymbol{U}_i^{(0)}$. A uniform gravitational force per unit mass $\boldsymbol{g}$ ($g = |\boldsymbol{g}|$) acts on the dispersion, and so

$$\boldsymbol{U}_i^{(0)} = \frac{2a_i^2(\rho_i - \rho)\boldsymbol{g}}{9\mu} \quad \text{and} \quad \boldsymbol{U}_j^{(0)} = \gamma\lambda^2 \boldsymbol{U}_i^{(0)},$$

where

$$\lambda = \frac{a_j}{a_i}, \quad \gamma = \frac{\rho_j - \rho}{\rho_i - \rho}.$$

The Reynolds number $R_i \equiv \rho|\boldsymbol{U}_i^{(0)}|a_i/\mu$ of each sphere is assumed to be small compared with unity.

2.1. *Expression for the relative velocity of two spheres*

For a dilute dispersion, the probability of a third particle influencing the relative motion of two interacting spheres is small, and so we only need consider pairwise interactions. We consider then a sphere of species j whose centre is at a position $\boldsymbol{r}$ ($r = |\boldsymbol{r}|$) relative to the centre of a sphere of species i. These two spheres move relative to one another due both to gravity and to an interparticle force of potential $\Phi_{ij}(r)$ which acts between them. Since inertia forces are negligible, the hydrodynamic force on each particle balances the applied force, and the velocity $\boldsymbol{V}_{ij} = \boldsymbol{U}_j - \boldsymbol{U}_i$ of sphere j relative to sphere i depends only on the relative position of the two spheres. An expression for this velocity has been presented by Batchelor (1982), the essential details of which are repeated here:

$$\boldsymbol{V}_{ij}(\boldsymbol{r}) = \boldsymbol{V}_{ij}^{(0)} \cdot \left\{ \frac{\boldsymbol{rr}}{r^2} L(s) + \left(\boldsymbol{I} - \frac{\boldsymbol{rr}}{r^2} \right) M(s) \right\} - \frac{D_{ij}^{(0)}}{kT} \left\{ \frac{\boldsymbol{rr}}{r^2} G(s) + \left(\boldsymbol{I} - \frac{\boldsymbol{rr}}{r^2} \right) H(s) \right\} \cdot \boldsymbol{\nabla}(\Phi_{ij}), \quad (2.1)$$

where $\boldsymbol{V}_{ij}^{(0)} = \boldsymbol{U}_j^{(0)} - \boldsymbol{U}_i^{(0)}$ is the relative velocity due to gravity of two widely separated spheres, and

$$\frac{D_{ij}^{(0)}}{kT} = \frac{1}{6\pi\mu}\left(\frac{1}{a_i} + \frac{1}{a_j}\right)$$

is the relative particle mobility of two widely separated spheres, with k Boltzmann's constant and T the absolute temperature. The particle mobility has been written in terms of the relative diffusivity $D_{ij}^{(0)}$ for convenience. The functions L and M depend only on λ, γ and the dimensionless distance $s = 2r/(a_i + a_j)$. These are unchanged when λ and γ are replaced by λ^{-1} and γ^{-1}, and when $\lambda = 1$ both L and M are independent of γ. The functions G and H depend only on λ and s, and they are unchanged when λ is replaced with λ^{-1}. Each of these functions is defined by Batchelor (1982) in terms of the two-sphere mobility functions. Numerical values of the mobility functions for arbitrary values of λ and s have been made available recently by Jeffrey & Onishi (1984).

Under conditions in which the spheres move relative to one another as a result of Brownian motion, there is an additional contribution to (2.1) equal to

$$D_{ij}^{(0)} \left\{ \frac{\boldsymbol{rr}}{r^2} G(s) + \left(\boldsymbol{I} - \frac{\boldsymbol{rr}}{r^2} \right) H(s) \right\} \cdot \boldsymbol{\nabla}(\log p_{ij}(\boldsymbol{r})),$$

where the pair-distribution function $p_{ij}(\boldsymbol{r})$ is the probability that a sphere of species j is at position $\boldsymbol{r}$ relative to a sphere of species i (p_{ij} being normalized so that $p_{ij} \to 1$ as $r \to \infty$). The magnitude of this term in comparison with the relative velocity due to gravity is measured by the inverse of the Péclet number

$$P_{ij} = \frac{1}{2}\frac{a_i + a_j}{D_{ij}^{(0)}} V_{ij}^{(0)},$$

where $V_{ij}^{(0)} = |\boldsymbol{V}_{ij}^{(0)}|$. Note that, for a given λ, P_{ij} is proportional to $(a_i + a_j)^4$. For typical hydrosols and aerosols, P_{ij} is large compared with unity when the radii of the particles are about 2 μm or larger. We shall consider only dispersions for which $P_{ij} \gg 1$ and shall neglect Brownian motion.

2.2. *The assumed interparticle force potential*

In hydrosol dispersions the interparticle force is the sum of an attractive van der Waals force and a repulsive electrical double-layer force. In aerosols there again is an attractive van der Waals force, and the particles may also carry electrical charges; however, the double layer of ions is not present, and the charges of two interacting particles may be either repulsive or attractive. When the repulsive force dominates, the particles remain dispersed, and the dispersion is said to be stable; when the attractive forces dominate, the dispersion is unstable and the particles flocculate. Our aim in this paper is to determine the rate at which coagulation occurs, and we shall consider only those dispersions whose interparticle force is dominated by the attractive van der Waals force.

The van der Waals force between two isolated particles was first calculated by Hamaker (1937) who assumed pairwise additivity of the intermolecular attractions. For unequal spheres, the force potential as a function of the separation distance is

$$\Phi_{ij} = -\frac{A}{6}\left[\frac{8\lambda}{(s^2-4)(1+\lambda)^2} + \frac{8\lambda}{s^2(1+\lambda)^2-4(1-\lambda)^2} + \log\left\{\frac{(s^2-4)(1+\lambda)^2}{s^2(1+\lambda)^2-4(1-\lambda)^2}\right\}\right], \quad (2.2a)$$

where A is the composite Hamaker constant for the materials composing the two spheres and the surrounding fluid medium. Its value should be determined experimentally or by the more rigorous theory of Lifshitz (1955). When the spheres are very close, $\xi \equiv s-2 \ll 1$ and $\xi \ll \lambda$, this expression reduces to

$$\Phi_{ij} = -\frac{A\lambda}{3(1+\lambda)^2\xi}. \quad (2.2b)$$

The Hamaker calculation neglected electromagnetic retardation and hence is valid only for separations less than the London wavelength λ_L, which is typically 0.1 μm. Retardation was included by Schenkel & Kitchner (1960) who reported the following best-fit approximations to their numerical integrations for equal-sized spheres and $\xi \ll 1$:

$$\Phi_{ij} = -\frac{A}{12\xi(1+11.2h/\lambda_L)} \quad \text{when} \quad \frac{h}{\lambda_L} \leqslant \pi, \quad (2.3a)$$

$$\Phi_{ij} = -\frac{10^{-3}A}{\xi}\left\{\frac{6.5}{h/\lambda_L} - \frac{0.305}{(h/\lambda_L)^2} + \frac{0.0057}{(h/\lambda_L)^3}\right\} \quad \text{when} \quad \frac{h}{\lambda_L} > \pi, \quad (2.3b)$$

where h is the gap between the spheres. When considering two spheres that are not of equal size, the right-hand side of (2.3) is multiplied by $4\lambda/(1+\lambda)^2$.

If we choose A as a measure of the strength of the van der Waals force, then the

magnitude of the relative velocity as a result of this force in comparison with that due to gravity is represented by the inverse of the parameter

$$Q_{ij} = \frac{\frac{1}{2}(a_i+a_j)\,V_{ij}^{(0)}}{AD_{ij}^{(0)}/kT} = \frac{2\pi|\rho_i-\rho|a_i^4\lambda|1-\gamma\lambda^2|g}{3A}. \tag{2.4}$$

This parameter is analogous to the inverse of the parameter H_A defined by Adler (1981) for the case where the two spheres are in relative motion resulting from an imposed bulk flow of the dispersion rather than from gravity. Also, note that $Q_{ij} = P_{ij}kT/A$, and, since kT/A is usually of order unity for hydrosols and of order 10^{-1} for aerosols, the restriction that P_{ij} is large will often require that Q_{ij} be large. In this case the effect of the van der Waals force is negligible unless the particles are very close. In light of (2.2*b*), $\mathrm{d}\Phi_{ij}/\mathrm{d}s$ behaves asymptotically as $\lambda A/(3(1+\lambda)^2\xi^2)$ as $\xi\to 0$. Furthermore, since L and G are each proportional to ξ for small ξ (Batchelor 1982), it is evident from (2.1) that the interparticle force will only be important within a thin boundary layer in which $\xi = O(Q_{ij}^{-\frac{1}{2}})$ or less; outside this boundary layer the relative motion is dominated by the gravitational term in (2.1). These facts will be exploited in §3 where an asymptotic solution for the trajectories defined by (2.1) will be presented for $Q_{ij} \gg 1$.

Finally, since Q_{ij} and P_{ij} are approximately of the same magnitude, the question arises as to whether Brownian motion might also become important in the boundary layer near $r = a_i+a_j$. However, since the boundary-layer thickness is of order $Q_{ij}^{-\frac{1}{2}}$, the relative velocity due to Brownian motion compared with that due to the van der Waals force is $O(Q_{ij}^{\frac{1}{2}}/P_{ij})$ in the boundary layer. This quantity is small for the conditions already stated.

2.3. *Expression for the collision rate*

The rate at which (i,j) doublets form in unit volume is equal to the flux of pairs into the contact surface $r = a_i+a_j$,

$$J_{ij} = -n_i n_j \int_{r=a_i+a_j} p_{ij}\,\boldsymbol{V}_{ij}\cdot\boldsymbol{n}\,\mathrm{d}A. \tag{2.5}$$

The pair-distribution function $p_{ij}(\boldsymbol{r})$ satisfies the conservation equation

$$\frac{\partial p_{ij}}{\partial t} + \boldsymbol{\nabla}\cdot(p_{ij}\,\boldsymbol{V}_{ij}) = 0. \tag{2.6}$$

For dilute dispersions, an approximate steady state is established. The divergence term in (2.6) is then equal to zero, and the integral in (2.5) may be taken over any surface enclosing the sphere $r = a_i+a_j$. When the spheres come into contact, we shall assume that a permanent doublet is formed (i.e. no rebound or subsequent separation occurs), and the boundary condition at the contact surface is therefore

$$p_{ij}(\boldsymbol{r}) = 0 \quad \text{for} \quad r = a_i+a_j. \tag{2.7a}$$

Provided all of the particle–particle encounters originate at very large separations, the other boundary condition is

$$p_{ij}(\boldsymbol{r})\to 1 \quad \text{as} \quad r\to\infty. \tag{2.7b}$$

We note that, in the absence of interparticle forces, a region of closed trajectories exists for certain values of λ and γ as discussed by Wacholder & Sather (1974) and by Batchelor & Wen (1982), and in these cases (2.7*b*) is inappropriate. For many of these

closed trajectories, however, the particles pass quite closely to one another, and, in the presence of an attractive force, these particles eventually coagulate. Only those trajectories which originate at infinite separation will be considered in the remainder of this study.

The expression for the collision rate in terms of the particle–particle trajectories is obtained by following the arguments of Zeichner & Schowalter (1977). The integral in (2.5) is taken over the surface which encloses the volume occupied by all the trajectories that originate at $r = \infty$ and terminate with the particles coming into contact. The cross section of this volume at $r = \infty$ is a circle of radius y_c^*, and, since $p_{ij} = 1$ and $V_{ij} = V_{ij}^{(0)}$ at $r = \infty$, the rate of doublet formation is then

$$J_{ij} = n_i n_j V_{ij}^{(0)} \pi (a_i + a_j)^2 E_{ij}, \tag{2.8}$$

where $E_{ij} \equiv y_c^{*2}/(a_i + a_j)^2$ is the collision efficiency. In the model by Smoluchowski (1917), E_{ij} has the value of unity. Our problem is now reduced to one of determining the parameter y_c^* which is equal to the largest horizontal displacement from the vertical axis of symmetry ($\boldsymbol{g}$ being in the vertical direction) possible for two widely separated spheres that eventually will collide. The path traced by one of these spheres relative to the other is called the limiting trajectory.

A second possible approach to our problem is to obtain a statistical description of the dispersion by solving (2.6) and (2.7) for the pair-distribution function everywhere in the region $a_i + a_j < r < \infty$. This solution can then be used in (2.5) to give the rate at which doublets are formed. Such a statistical description of the dispersion was used in the calculation by Batchelor (1982) and Batchelor & Wen (1982) of the mean sedimentation velocity of small particles in a dilute suspension, and it is needed when Brownian diffusion is important. In some recent work, Wen & Batchelor (1984) have in fact used an analytic solution for the pair-distribution function to compute the rate of doublet formation in a dilute dispersion of particles having negligible inertia at large Péclet numbers. However, they were able to obtain only asymptotic results (for $Q_{ij} \gg 1$) similar to those given in § 3. I began the present work at the suggestion of Professor Batchelor with the intention of investigating the influence of the inertia of the particles on their collision rate by using a deterministic approach in which particle–particle trajectories were calculated. We subsequently realized that, in the absence of Brownian motion, the numerical trajectory analysis also allowed the calculation of the collision rate when the particle inertia is negligible at all values of Q_{ij} and so provided a simpler and more powerful method than the analytic solution for the pair-distribution function. I am, therefore, indebted to Professor Batchelor and to Dr Wen for providing much of the motivation for my work and for showing me their calculations.

3. Asymptotic solution for large Q_{ij}

We begin by decomposing the relative velocity given by (2.1) into the components along and normal to the line of centres, which in dimensionless form are respectively

$$u_r = \frac{\mathrm{d}s}{\mathrm{d}\tau} = -L(s)\cos\theta - \frac{G(s)}{Q_{ij}}\frac{\mathrm{d}\phi_{ij}}{\mathrm{d}s} \tag{3.1a}$$

and

$$u_\theta = s\frac{\mathrm{d}\theta}{\mathrm{d}\tau} = M(s)\sin\theta. \tag{3.1b}$$

The velocities have been made dimensionless with $V_{ij}^{(0)}$;

$$\tau = 2V_{ij}^{(0)}t/(a_i+a_j), \quad \phi_{ij} = \Phi_{ij}/A,$$

and θ is the angle between $\boldsymbol{g}$ and $\boldsymbol{r}$.

3.1. *The outer region*

When $Q_{ij} \gg 1$ the van der Waals force is negligible outside a boundary layer near $s = 2$, and the relative motion of the two spheres is due to gravity only. We eliminate time by applying the chain rule to (3.1), which yields the trajectory equation

$$\frac{\mathrm{d}s}{\mathrm{d}\theta} = -\frac{sL(s)}{M(s)}\cot\theta. \tag{3.2}$$

The initial condition for this equation is

$$s\sin\theta = y_\infty \quad \text{for} \quad s\to\infty, \tag{3.3}$$

where y_∞ is the horizontal displacement of the spheres when they are widely separated. Since (3.2) is separable, the solution subject to (3.3) is immediately found to be

$$Y(s) \equiv \frac{y_\infty}{s\sin\theta} = \exp\left\{\int_s^\infty \frac{(L-M)}{sL}\,\mathrm{d}s\right\}. \tag{3.4}$$

We note here that y_∞^2 can be thought of as the stream function for the particle motion since it is a conserved quantity along particle trajectories, and it is directly proportional to the flux of particle pairs between the trajectory defined by y_∞ = constant and the stagnation trajectory $y_\infty = 0$. Furthermore, by comparing the above with the analysis of Batchelor (1982), we find that $Y(s) = (p_{ij}(s)\,L(s))^{\frac{1}{2}}$. This provides a very simple relationship between the deterministic trajectories in the outer region and the statistical pair-distribution function.

When the spheres are very close ($\xi \ll 1$ and $\xi \ll \lambda$), the mobility functions have the asymptotic forms given by Jeffrey & Onishi (1984), and we can deduce from these that

$$L(s) \sim L_1\xi + O(\xi^2\log\xi^{-1}) \tag{3.5a}$$

and

$$M(s) \sim \frac{a_1(\log\xi^{-1})^2 + a_2\log\xi^{-1} + a_3}{(\log\xi^{-1})^2 + e_1\log\xi^{-1} + e_2} + O(\xi(\log\xi^{-1})^3). \tag{3.5b}$$

The simplified asymptotic form of (3.5*b*),

$$M(s) \sim a_1 + \frac{a_2 - e_1a_1}{\log\xi^{-1}},$$

that has been used on occasion in other applications proves to be of insufficient accuracy for the values of ξ that are important for the current purpose.

When we substitute (3.5) into (3.4), we find that the form of the trajectories when the particles become close is

$$Y(s) \sim \frac{y_\infty}{2\sin\theta} \sim \frac{k_1\xi^{b_1}}{[(\log\xi^{-1})^2 + e_1\log\xi^{-1} + e_2]^{b_2}\left[\dfrac{e_1 + 2\log\xi^{-1} + \Delta}{e_1 + 2\log\xi^{-1} - \Delta}\right]^{b_3}}, \tag{3.6}$$

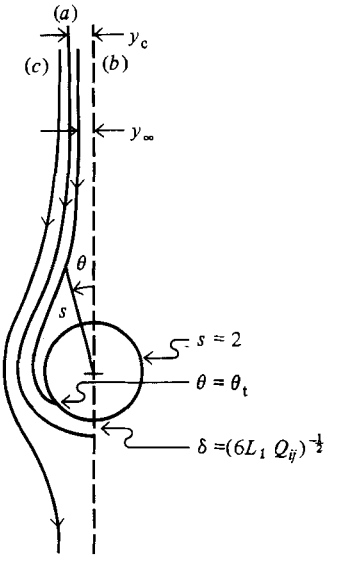

FIGURE 1. Schematic showing the relative trajectories of the centres of two spheres: (*a*) the limiting trajectory; (*b*) a trajectory terminating with contact; (*c*) a trajectory in which the spheres move past one another and separate (not to scale).

where

$$b_1 = \frac{a_1}{2L_1}, \quad b_2 = \frac{a_2 - e_1 a_1}{4L_1},$$

$$b_3 = \frac{e_1 a_2 - 2a_3 - a_1(e_1^2 - 2e_2)}{4L_1 \Delta}, \quad \Delta = (e_1^2 - 4e_2)^{\frac{1}{2}}.$$

The constant k_1 is obtained from matching the numerical evaluation of (3.4) with this asymptotic form.

3.2. *The boundary-layer region*

When the gravitational force has brought the two particles to within a distance of $\xi = O(Q_{ij}^{-\frac{1}{2}})$ of each other, the van der Waals force begins to draw them together. For $Q_{ij} \gg 1$ this distance is very small, and we expect that (3.5) provides an adequate approximation for L and M. Furthermore, when $\xi \ll 1$ and $\xi \ll \lambda$,

$$\phi_{ij}(s) \sim \frac{-\lambda}{3(1+\lambda)^2 \xi} + O(\log \xi^{-1}) \quad \text{and} \quad G(s) \sim \frac{(1+\lambda)^2}{2\lambda} \xi + O(\xi^2 \log \xi^{-1}). \quad (3.7), (3.8)$$

In this case, the equations for the relative velocity of the two spheres are

$$\frac{\mathrm{d}\xi}{\mathrm{d}\tau} = -L_1 \xi \cos\theta - \frac{1}{6Q_{ij}\xi} \quad (3.9a)$$

and

$$\frac{\mathrm{d}\theta}{\mathrm{d}\tau} = \frac{\{a_1(\log \xi^{-1})^2 + a_2 \log \xi^{-1} + a_3\} \sin\theta}{2\{(\log \xi^{-1})^2 + e_1 \log \xi^{-1} + e_2\}}. \quad (3.9b)$$

For the time being we are neglecting retardation effects; this is appropriate provided that $\xi \ll 2\lambda_L/(a_i + a_j)$. Retardation may be included in the analysis simply by using (2.3) in place of (3.7).

The relative velocity of the two spheres is zero when $\theta = \pi$ and $\xi = (6L_1 Q_{ij})^{-\frac{1}{2}}$. In this configuration one sphere is directly below the other, and the attractive van der Waals force just balances the gravitational force which acts to pull the spheres apart. Moreover, this configuration is the termination point of the limiting trajectory; particle pairs that are on the inside of this limiting trajectory will eventually come into contact, whereas those on the outside will move past one another and separate (see figure 1).

The collision parameter $y_c = 2y_c^*/(a_i + a_j)$ is determined by integrating backwards along the limiting trajectory from the termination point $\theta = \pi$ and $\xi = (6L_1 Q_{ij})^{-\frac{1}{2}}$, and then matching the solution with (3.6) when ξ has become sufficiently large so that the van der Waals force no longer influences the particle paths. An appropriate scaling of the particle separation in the boundary layer is evidently $\eta = \xi/\delta$, where $\delta = (6L_1 Q_{ij})^{-\frac{1}{2}}$ is a measure of the boundary-layer thickness. In terms of this boundary-layer coordinate, the trajectory equation found from dividing (3.9*a*) by (3.9*b*) is

$$\frac{\mathrm{d}\eta}{\mathrm{d}\theta} = \frac{-2L_1(\eta^2 \cos\theta + 1)}{\eta \sin\theta \left\{\dfrac{a_1(\log(\eta\delta))^2 + a_2 \log(\eta\delta)^{-1} + a_3}{(\log(\eta\delta))^2 + e_1 \log(\eta\delta)^{-1} + e_2}\right\}}. \tag{3.10}$$

We shall integrate (3.10) numerically from the point $\eta = 1$, $\theta = \pi$ in the direction of decreasing θ. Analytically we find that when $\eta \gg 1$

$$\frac{\eta^{b_1} \sin\theta}{\{(\log(\eta\delta))^2 + e_1 \log(\eta\delta)^{-1} + e_2\}^{b_2} \left\{\dfrac{e_1 + 2\log(\eta\delta)^{-1} + \Delta}{e_1 + 2\log(\eta\delta)^{-1} - \Delta}\right\}^{b_3}} = \frac{k_2}{\{(\log\delta)^2 + e_1 \log\delta^{-1} + e_2\}^{b_2} \left\{\dfrac{e_1 + 2\log\delta^{-1} + \Delta}{e_1 + 2\log\delta^{-1} - \Delta}\right\}^{b_3}}. \tag{3.11}$$

The value of k_2 is determined from the numerical integration of (3.10). The denominator in the right-hand side of (3.11) has been included so that k_2 is only a very weak function of Q_{ij}, tending to a constant for very large values of Q_{ij} (see table 1).

3.3. *The expression for the collision efficiency*

In a region of overlap defined by $\delta \ll \xi \ll 1$ the shape of the trajectory in the boundary layer as given by (3.11) matches with that given by (3.6) for the trajectory in the outer region. Since $y_\infty = y_c$ for the limiting trajectory, the collision efficiency found from equating these two expressions is

$$E_{ij} = \tfrac{1}{4} y_c^2 = \frac{(k_1 k_2)^2}{(6L_1 Q_{ij})^{b_1} \{(\frac{1}{2}\log(6L_1 Q_{ij})^2 + \frac{1}{2} e_1 \log(6L_1 Q_{ij}) + e_2\}^{2b_2} \left\{\dfrac{e_1 + \log(6L_1 Q_{ij}) + \Delta}{e_1 + \log(6L_1 Q_{ij}) - \Delta}\right\}^{2b_3}}. \tag{3.12}$$

We note that this can be written in the form $E_{ij} = c\delta p_{ij}(\delta)$, where $c = k_2^2 L_1$ is a slowly varying function of Q_{ij}, and $p_{ij}(\delta)$ is the pair-distribution function from the outer region evaluated at $\xi = \delta$. This form has the satisfying interpretation that the number of collisions that take place (ultimately as a result of the van der Waals force) is

λ	γ	L_1	b_1	b_2	b_3	e_1	e_2	k_1	k_2	Q_{ij}
0.9	1.0	0.775	0.242	0.262	−0.03	6.04	6.30	0.862	1.28	10^2
									1.25	10^4
									1.23	10^6
0.5	1.0	0.635	0.118	0.426	0.320	5.63	4.27	1.50	1.29	10^2
									1.25	10^4
									1.23	10^6
0.25	1.0	0.394	0.060	0.699	0.615	3.84	0.46	2.45	1.35	10^2
									1.27	10^4
0.125	1.0	0.217	0.021	0.779	0.696	1.61	−1.38	1.39	1.49	10^3
									1.37	10^4
									1.31	10^5
1.0	$\gamma \neq 1$	2.0	0.100	0.067	−0.07	6.07	6.39	0.725	1.16	10^2
									1.15	10^4
									1.15	10^6

TABLE 1. Values of the constants that appear in (3.12) – the asymptotic expression for the collision efficiency – for $\gamma = 1$ and $\lambda = 0.125$, 0.25, 0.5 and 0.9, and for $\lambda = 1$ and arbitrary γ

proportional to the number of particle pairs that reach the boundary layer as a result of the gravitational force. This result was also found by Wen & Batchelor (1984), only with the values of c varying slightly from the present analysis owing to the different approximations made.

The constants that appear in (3.12) are presented in table 1 for $\gamma = 1$ and $\lambda = 0.125$, 0.25, 0.5, and 0.9, and for $\lambda = 1$ and arbitrary γ (provided that $\gamma \neq 1$). These results are unchanged when λ and γ are replaced by λ^{-1} and γ^{-1}. Recall that, when $\lambda = 1$, L and M are independent of γ; hence the collision efficiency as a function of the parameter Q_{ij} is also independent of γ when $\lambda = 1$. Figure 2 is a plot of E_{ij} versus Q_{ij} for these cases. In general, E_{ij} is very small owing to the large hydrodynamic resistance, which prevents the close approach of the two spheres. As Q_{ij} increases, the gap between the two spheres for which the attractive van der Waals force becomes important decreases, and E_{ij} decreases. Also, the collision efficiency is even lower when one sphere is much smaller than the other, because then the smaller sphere tends to follow the streamlines of the flow around the larger sphere, and close contact is not made unless the smaller sphere is on a streamline which begins very close to the vertical axis of symmetry. This decrease in E_{ij} for small λ was also found by Adler (1981) for the case of heterocoagulation of spheres in simple shear flow, and will be considered in more detail in §3.4.

The dashed lines in figure 2 are the asymptotic results given by (3.12), whereas the solid lines are from numerical computations of the limiting trajectory using the complete forms of $L(s)$, $M(s)$ and $G(s)$ in (3.1), and also using (2.2a) for the van der Waals potential. The asymptotic results are in excellent agreement with the complete numerical results when $Q_{ij} > 10^2$. In fact, for cases (b) and (c), the asymptotic curves and the exact numerical curves coincide over the entire range of Q_{ij} presented, and for the remaining curves the error in the asymptotic approximation is at most 10% when $Q_{ij} = 10$. This close agreement is surprising in light of the fact that the error in the asymptotic theory should increase with $\delta = (6L_1 Q_{ij})^{-\frac{1}{2}}$. A careful examination

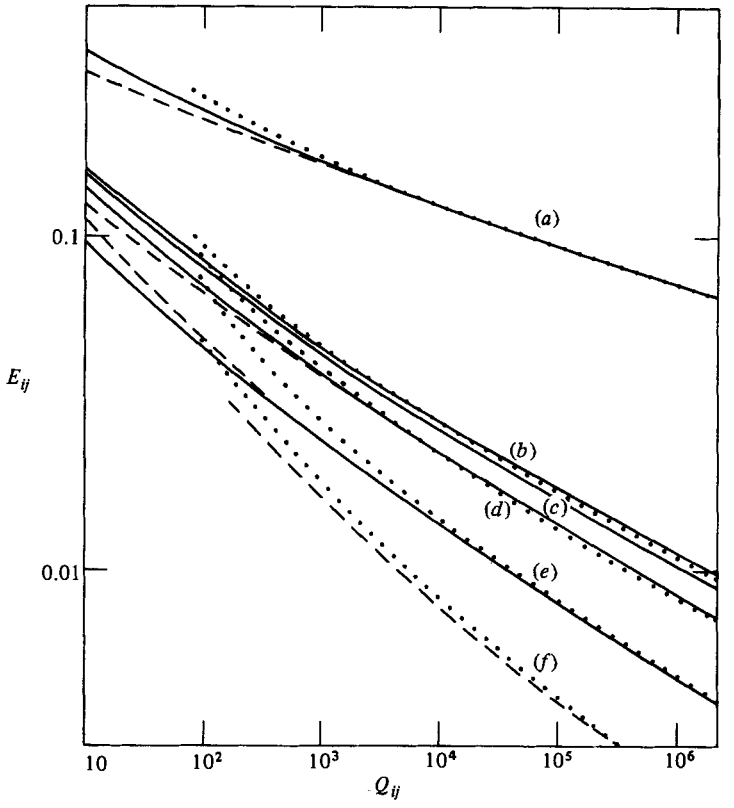

FIGURE 2. The collision efficiency as a function of the parameter Q_{ij} for zero particle inertia and for (*a*) $\lambda = 1$, $\gamma \neq 1$ (arbitrary); (*b*) $\gamma = 1$, $\lambda = 0.9$; (*c*) $\gamma = 1$, $\lambda = \frac{3}{4}$; (*d*) $\gamma = 1$, $\lambda = \frac{1}{2}$; (*e*) $\gamma = 1$, $\lambda = \frac{1}{4}$; (*f*) $\gamma = 1$, $\lambda = \frac{1}{8}$. The dashed lines are the asymptotic results given by (3.12); the solid lines are from the complete numerical solution of (3.1); the dotted lines are reproduced from Wen & Batchelor (1984).

of the asymptotic analysis reveals that some of the approximations lead to an overestimation of the collision efficiency, whereas others lead to an underestimation of the collision efficiency. These competing effects fortuitously tend to cancel each other, which explains the better than expected agreement between the asymptotic and exact results; this also explains the fact that in some cases the asymptotic curves approach the exact results from above and in other cases from below. The dotted lines in figure 2 are reproduced from Wen & Batchelor (1984). These asymptotic results, obtained in a very different manner, are in close agreement with the present results, provided that $Q_{ij} > 10^3$. For smaller Q_{ij} the collision efficiencies determined by the two techniques begin to diverge, which is not surprising considering the different approximations made.

3.4. *The limits* $\lambda \to 1$ *and* $\lambda \to 0$

When $\lambda = 1$ the relative trajectory of the two spheres is independent of γ (provided that $\gamma \neq 1$), and the collision efficiency is given by curve (*a*) in figure 2. On the other hand, it is evident also from figure 2 that the curve corresponding to the limit $\gamma = 1$, $\lambda \to 1$ must be very close to the one for $\gamma = 1$, $\lambda = 0.9$ – and hence quite different from that for $\lambda = 1$ and arbitrary γ. When $\gamma = 1$ and $\lambda \to 1$ the relative trajectory of the

two spheres approaches a limiting shape, but this shape is not the same as the shape of the trajectory for $\lambda = 1$ and $\gamma \to 1$. The existence of the different trajectories in these two limits is the essential reason for the different collision efficiencies. Of course $V_{ij}^{(0)} = |(1-\gamma\lambda^2)\, U_i^{(0)}|$, and the relative velocity at which the particles traverse these trajectories decreases towards zero when $\lambda \to 1$ and $\gamma \to 1$; hence Q_{ij} decreases in the same manner, and E_{ij} increases (the particles spend more time in close proximity, thereby giving the van der Waals force a greater chance to bring them together). It should be remembered that $V_{ij}^{(0)} = 0$ when λ and γ are each exactly unity, and Brownian diffusion is then dominant. For the present analysis to apply, either λ or γ, or both, must differ sufficiently from unity so that P_{ij} is large.

When $\lambda \to 0$ the situation is quite different from that discussed so far. In this case the smaller sphere follows the fluid streamlines as it moves around the larger sphere, and we have (see §2 in Batchelor 1982)

$$L(s) \doteq 1-3s^{-1}+4s^{-3}+O(\lambda) \quad \text{and} \quad M(s) = 1-\tfrac{5}{2}s^{-1}-2s^{-3}+O(\lambda). \quad (3.13a,b)$$

These expressions have the asymptotic forms for $\lambda \ll \xi \ll 1$ of

$$L(s) \sim \tfrac{3}{8}\xi^2+O(\xi^3)+O(\lambda\xi) \quad \text{and} \quad M(s) \sim \tfrac{3}{4}\xi+O(\xi^2)+O(\lambda). \quad (3.14a,b)$$

When $r-(a_i+a_j)$ is comparable to or smaller than the radius of the smaller sphere, (3.13) and (3.14) do not apply. However, as we shall see, for sufficiently small λ the van der Waals force is strong enough to draw in the smaller sphere even when its distance from the larger sphere is several times its own radius. As $\lambda \to 0$ the van der Waals force is equal to that of a sphere near a plane, and for negligible retardation this is

$$\frac{\mathrm{d}\phi_{ij}}{\mathrm{d}s} = \frac{16\lambda^3}{3\xi^2(4\lambda+\xi)^2}. \quad (3.15)$$

Also, when $\lambda \ll \xi \ll 1$, $G(s) \sim 1$, and the interparticle force balances the gravitational force exactly at the point

$$\theta = \pi, \quad \xi = \delta' = \left(\frac{128\lambda^2}{9Q_{ij}}\right)^{\frac{1}{6}}.$$

The limiting trajectory can be found as before by considering an outer region in which the interparticle force is negligible ($\xi \gg \delta'$) and an inner region where $\xi = O(\delta')$. The final result for the collision efficiency is found to be simply

$$E_{ij} = \frac{1.69\lambda}{Q_{ij}^{\frac{1}{3}}}. \quad (3.16)$$

Since Q_{ij} is proportional to λ, E_{ij} is proportional to $\lambda^{\frac{2}{3}}$ for small λ. This result is of only limited practical importance since it applies only when $P_{ij} = Q_{ij}A/kT$ is large compared with unity and λ is sufficiently small so that the condition $\lambda \ll \delta' \ll 1$ is satisfied.

3.5. *Distribution of capture sites*

In the preceding sections we computed the collision rate by examining the limiting trajectory. In some applications we may be interested in knowing not only the rate at which collisions take place but also the distribution of locations on the particle surfaces where contact occurs. The capture-site distribution may be computed directly from our trajectory analysis. Instead of integrating (3.10) starting at the termination point of the limiting trajectory, we start at the termination point of a trajectory ending in contact, namely $\eta = 0$ for some $\theta = \theta_t$ (see figure 1). After

integrating (3.10) in the direction of decreasing θ, the resulting trajectory is matched with the outer solution, and this yields the value of y_∞ for the trajectory with contact at $\theta = \theta_t$. The fraction of the collisions that occurs at values of θ less than θ_t is $(y_\infty/y_c)^2$.

For $\lambda = \frac{1}{4}$, $\gamma = 1$ and $Q_{ij} = 10^{-5}$ I found that 34.5% of the collisions occur in the range of $0 \leqslant \theta_t < \frac{1}{4}\pi$, 52.08% in the range $\frac{1}{4}\pi \leqslant \theta_t < \frac{1}{2}\pi$, 13.3% in the range $\frac{1}{2}\pi \leqslant \theta_t < \frac{3}{4}\pi$, and only 0.2% in the range $\frac{3}{4}\pi < \theta_t < \pi$. In other words, the majority of the collisions take place on the front hemispheres of the particles, and only a small percentage of the spheres travel around to the back of another sphere before being captured. The percentages listed above are typical of several calculations of the capture-site distribution for various Q_{ij} and λ (all with $\gamma = 1$).

4. The effects of particle inertia

When the particles are sufficiently massive, their inertia must be included when determining their trajectories, and the hydrodynamic forces no longer balance the applied forces. Also, the torque on the particles is non-zero. Instead, the net force and torque on each particle equal respectively its rate-of-change of linear momentum and angular momentum. We shall restrict our attention to dispersions in which the inertia of the surrounding fluid remains small, and so the hydrodynamic forces and torques are linear functions of the translational and rotational velocities of the particles. For convenience, we consider the translational motion of the two particles as being composed of their relative velocity and the velocity of the centre of mass of the pair. The momentum equations for the two-particle system, made dimensionless with $V_{ij}^{(0)}$ and $\frac{1}{2}(a_i + a_j)$ as the characteristic velocity and length respectively, are then

$$S\frac{d\boldsymbol{v}_{cm}}{d\tau} = f_{cm}\frac{\boldsymbol{g}}{g} + \left\{d_1\frac{\boldsymbol{rr}}{r_2} + d_2\left(\boldsymbol{I} - \frac{\boldsymbol{rr}}{r^2}\right)\right\}\cdot\boldsymbol{v}_{cm} + \left\{d_3\frac{\boldsymbol{rr}}{r^2} + d_4\left(\boldsymbol{I} - \frac{\boldsymbol{rr}}{r^2}\right)\right\}\cdot\boldsymbol{v}_{ij} + d_5\frac{\boldsymbol{r}}{r}\times\boldsymbol{\omega}_i + d_6\frac{\boldsymbol{r}}{r}\times\boldsymbol{\omega}_j, \quad (4.1a)$$

$$S\frac{d\boldsymbol{v}_{ij}}{d\tau_{ij}} = f_{ij}\frac{\boldsymbol{g}}{g} + \left\{d_7\frac{\boldsymbol{rr}}{r^2} + d_8\left(\boldsymbol{I} - \frac{\boldsymbol{rr}}{r^2}\right)\right\}\cdot\boldsymbol{v}_{cm} + \left\{d_9\frac{\boldsymbol{rr}}{r^2} + d_{10}\left(\boldsymbol{I} - \frac{\boldsymbol{rr}}{r_2}\right)\right\}\cdot\boldsymbol{v}_{ij} + d_{11}\frac{\boldsymbol{r}}{r}\times\boldsymbol{\omega}_i + d_{12}\frac{\boldsymbol{r}}{r}\times\boldsymbol{\omega}_j, \quad (4.1b)$$

$$S\frac{d\boldsymbol{\omega}_i}{d\tau} = d_{13}\frac{\boldsymbol{r}}{r}\times\boldsymbol{v}_{cm} + d_{14}\frac{\boldsymbol{r}}{r}\times\boldsymbol{v}_{ij} + d_{15}\boldsymbol{\omega}_i + d_{16}\boldsymbol{\omega}_j, \quad (4.1c)$$

$$S\frac{d\boldsymbol{\omega}_j}{d\tau} = d_{17}\frac{\boldsymbol{r}}{r}\times\boldsymbol{v}_{cm} + d_{18}\frac{\boldsymbol{r}}{r}\times\boldsymbol{v}_{ij} + d_{19}\boldsymbol{\omega}_i + d_{20}\boldsymbol{\omega}_j, \quad (4.1d)$$

where $\boldsymbol{v}_{cm}$ is the velocity of the centre of mass, and $\boldsymbol{\omega}_i$ and $\boldsymbol{\omega}_j$ are the angular velocities of sphere i and sphere j. The Stokes number is defined by

$$S = \frac{2V_{ij}^{(0)}(m_i m_j)^{\frac{1}{2}}}{3\pi\mu(a_i + a_j)^2}, \quad (4.2)$$

with $m_i = \frac{4}{3}\pi\rho_i a_i^3$ being the mass of sphere i, and similarly for sphere j. Also, the gravitational force coefficients are

$$f_{cm} = \frac{2(1+\gamma\lambda^3)(\beta\lambda^3)^{\frac{1}{2}}}{(1+\lambda)(1-\gamma\lambda^2)}, \quad f_{ij} = \frac{2(\gamma/\beta - 1)(\beta\lambda^3)^{\frac{1}{2}}}{(1+\lambda)(1-\gamma\lambda^2)(1+\beta\lambda^3)}.$$

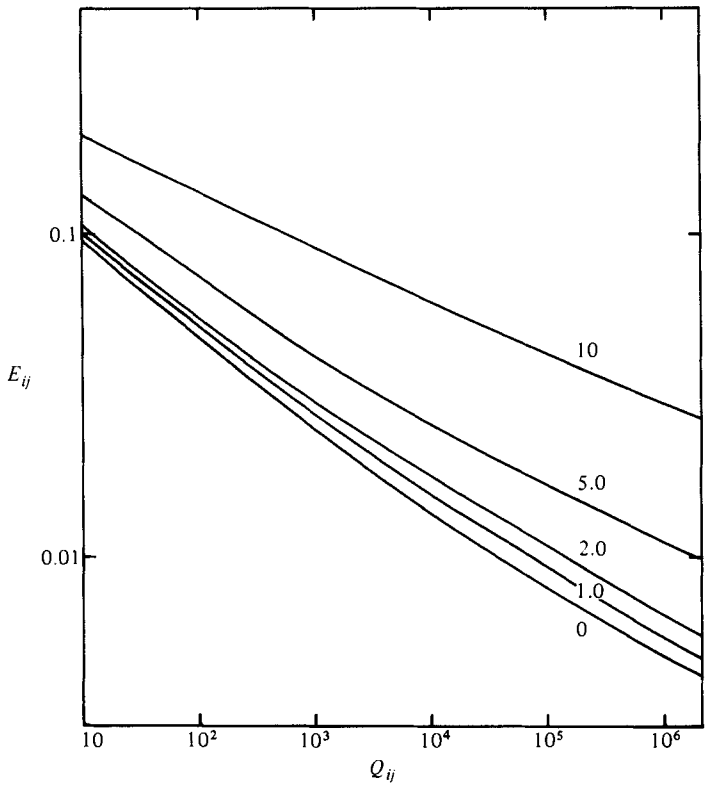

FIGURE 3. The collision efficiency as a function of the parameter Q_{ij} for $\gamma = 1$, $\lambda = \frac{1}{4}$, and $S = 0$, 1, 2, 5 and 10.

where $\beta \equiv \rho_j/\rho_i$. The coefficients $d_1, \ldots, d_{20}$ are functions of s and can be computed directly from the two-sphere resistance functions given by Jeffrey & Onishi (1984). In general, $d_1, \ldots, d_{20}$ also depend on the parameters λ, γ and β. The equation for the relative position of the two spheres is

$$\frac{\mathrm{d}\boldsymbol{s}}{\mathrm{d}\tau} = \boldsymbol{v}_{ij}, \tag{4.3}$$

where $\boldsymbol{s} \equiv \boldsymbol{r}/r$, which, along with (4.1) and the initial condition that the two spheres move with their terminal settling velocities when they are far apart, suffices to determine the relative trajectory of the pair. We note that the inertia parameter S is equal to the ratio of the relaxation time for the particle pair (i.e. the time that it takes one of the spheres to respond to changes in the flow caused by the presence of the other sphere) to the time that it takes the spheres to move a distance relative to each other that is equal to the sum of their radii. When $S = 0$ the particles follow the trajectories computed in §3; as S increases from zero, the particles deviate from these trajectories – they tend to move in straight lines rather than flow around each other. Thus we expect the collision efficiency to increase as the Stokes number increases. We also note that the Stokes number is proportional to the particle density, whereas the Reynolds number is proportional to the fluid density. Therefore, only when the particle density is much greater than the fluid density may the particle

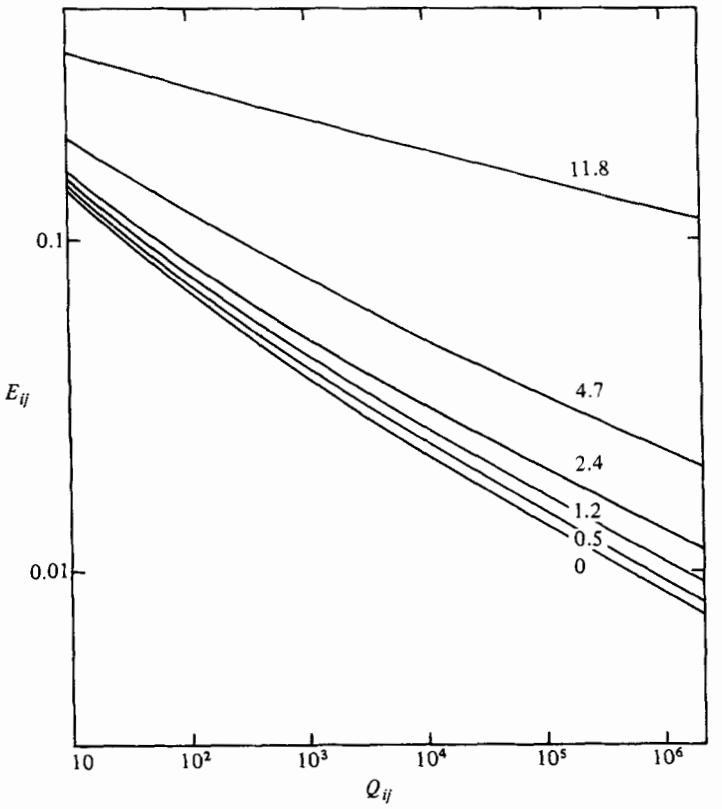

FIGURE 4. The collision efficiency as a function of the parameter Q_{ij} for $\gamma = 1$, $\lambda = \frac{1}{2}$, and $S = 0$, 0.5, 1.2, 2.4, 4.7 and 11.8.

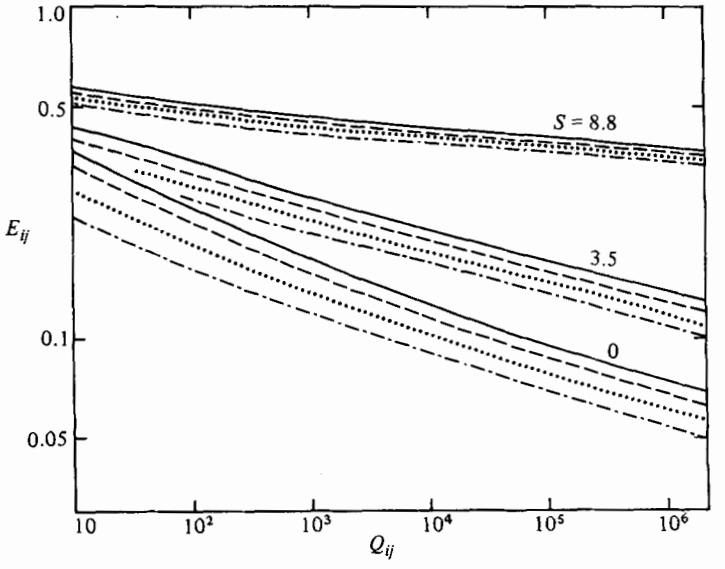

FIGURE 5. The collision efficiency as a function of the parameter Q_{ij} for $\lambda = 1$, $\beta = \gamma = \frac{1}{2}$, and $S = 0$, 3.5 and 8.8: ——, unretarded van der Waals force ($\epsilon_R = 0$); – – – –, $\epsilon_R = 0.2$; - - -, 1.0; –·–·–·, 5.0.

inertia be significant while the fluid inertia remains negligible. This is true, for example, in aerosol dispersions but not in hydrosol dispersions.

The trajectory equations (4.1) and (4.3) were integrated numerically using a fourth-order Runge–Kutta scheme with a variable time step. The asymptotic forms of the resistance functions for widely separated spheres given by Jeffrey & Onishi (1984) were used for $s > 4$, and the nearly touching expressions of Jeffrey & Onishi were used for $\xi = s-2 < 0.01$. In the intermediate range the resistance functions, correct to four figures, were computed by interpolating between pretabulated values. When the two spheres became close I found that the time step needed to be smaller than approximately ξS in order for the solution to remain stable. This difficulty was overcome by noting that the radial component of the relative velocity v_r is $O(\xi)$ when $\xi \ll 1$ (the coefficient d_9 has a ξ^{-1} singularity when $\xi \to 0$). The term $\mathrm{d}v_r/\mathrm{d}\tau$ is then also $O(\xi)$ in this range, and $S\,\mathrm{d}v_r/\mathrm{d}\tau$ can be neglected relative to the other terms in the radial component of (4.1*b*) when $S\xi \ll 1$. I included a switch in the program that reduced the order of the radial component of (4.1*b*) by setting $S\,\mathrm{d}v_r/\mathrm{d}\tau$ equal to zero for $S\xi < \epsilon$ (typically $\epsilon = 0.02$ was adequate). This equation was then rearranged to give an explicit expression for v_r in terms of the other variables. In general, three or four trajectories were computed for each case before the parameter y_c that defines the limiting trajectory was found accurate to three figures. The results of these computations are shown in figures 3–5, where the collision efficiency is plotted as a function of the parameter Q_{ij} for various values of the Stokes number and for (λ, γ, β) equal to $(\frac{1}{4}, 1, 1)$ $(\frac{1}{2}, 1, 1)$ and $(1, \frac{1}{2}, \frac{1}{2})$ respectively. The results are unchanged when λ, γ and β are replaced by λ^{-1}, γ^{-1} and β^{-1}. For $S = 0$ the collision efficiencies agree with the asymptotic results of §3; as S increases, E_{ij} of course increases, and also the slope of the curve E_{ij} versus Q_{ij} moves towards zero. We expect as $S \to \infty$ that the particle paths will become straight lines independent of one another, and the Smoluchowski result of $E_{ij} = 1$ will be obtained.

The effect of retardation of the interparticle force as given by (2.3) on the collision efficiency is also shown in figure 5. The retardation parameter ϵ_R is defined as the ratio of the boundary-layer thickness to the London wavelength, i.e.

$$\epsilon_R = \frac{(6L_1 Q_{ij})^{-\frac{1}{2}}}{2\lambda_L/(a_i + a_j)}.$$

When ϵ_R is small compared with unity, the electromagnetic retardation is negligible within the boundary layer where the van der Waals force is important. On the other hand, when ϵ_R is large the van der Waals force is severely retarded, and this lowers the collision efficiency. We see from figure 5 that when $\epsilon_R = 1.0$ and $S = 0$ the collision efficiency is reduced by about 25% from the unretarded case. Values for ϵ_R of order unity are not uncommon in practice, and the retarded interparticle force potential should then be used. Finally, as the Stokes number is increased the effect of retardation is reduced because the inertia of the particles brings them closer together.

5. Application to typical hydrosols and aerosols

We have seen in §3 that the collision efficiency E_{ij} decreases as the parameter Q_{ij} increases, and in §4 that E_{ij} increases as the Stokes number S increases. For a given fluid–particle system, however, Q_{ij} and S do not vary independently. In fact, both Q_{ij} and S increase as the radii of the particles increase, and so E_{ij} may either increase or decrease when the particle radii increase. In order for us to gain a better understanding of the coagulation process, the collision efficiency as a function of the

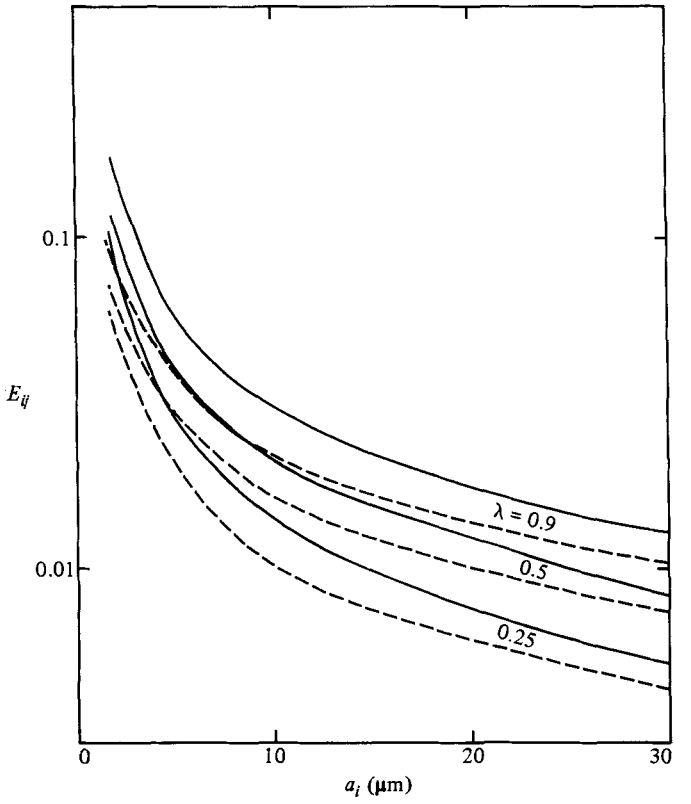

FIGURE 6. The collision efficiency as a function of the radius of the larger sphere for a typical hydrosol; $\mu = 0.01$ P, $\rho = 1.0$ g cm^{-3}, $\rho_i = \rho_j = 2\rho$ and $A = 5 \times 10^{-14}$ erg: ——, unretarded van der Waals force; – – – –, retarded van der Waals force.

radius of the larger sphere has been computed for a typical hydrosol dispersion and for a typical aerosol dispersion.

5.1. *The collision efficiency for a hydrosol dispersion*

For the hydrosol we choose the values $\mu = 0.01$ P, $\rho = 1.0$ g cm^{-3}, $\rho_i = \rho_j = 2\rho$, $A = 5 \times 10^{-14}$ erg and $kT = 4 \times 10^{-14}$ erg. In this case $P_{ij} = 1.25 Q_{ij}$, and, when $\lambda = \frac{1}{2}$, for example, P_{ij} is greater than 10 provided that $a_i \geqslant 1.5$ μm, and R_i is less than 0.1 provided that $a_i \leqslant 35$ μm. Also, for these conditions, $S = 0.10 R_i$, and the inertia of the particles is negligible. We then expect that E_{ij} will decrease monotonically with increasing a_i, and this is shown in figure 6 for $\lambda = \frac{1}{4}$, $\frac{1}{2}$ and 0.9. The solid lines correspond to the unretarded van der Waals potential, and the dashed lines are for the retarded van der Waals potential. In general, the collision efficiency is very low. When $a_i \geqslant 10$ μm the simple Smoluchowski impact model ($E_{ij} = 1$) overestimates the rate of coagulation of a dilute sedimenting suspension by about two orders of magnitude.

5.2. *The collision efficiency for an aerosol dispersion*

In contrast with hydrosols, we expect particle inertia to play a significant role in the coagulation of aerosols. For a typical aerosol system, we choose $\mu = 1.7 \times 10^{-4}$ P, $\rho = 1.3 \times 10^{-3}$ g cm^{-3}, $\rho_i = \rho_j = 1.0$ g cm^{-3}, $A = 5 \times 10^{-13}$ erg and $kT = 4 \times 10^{-14}$ erg

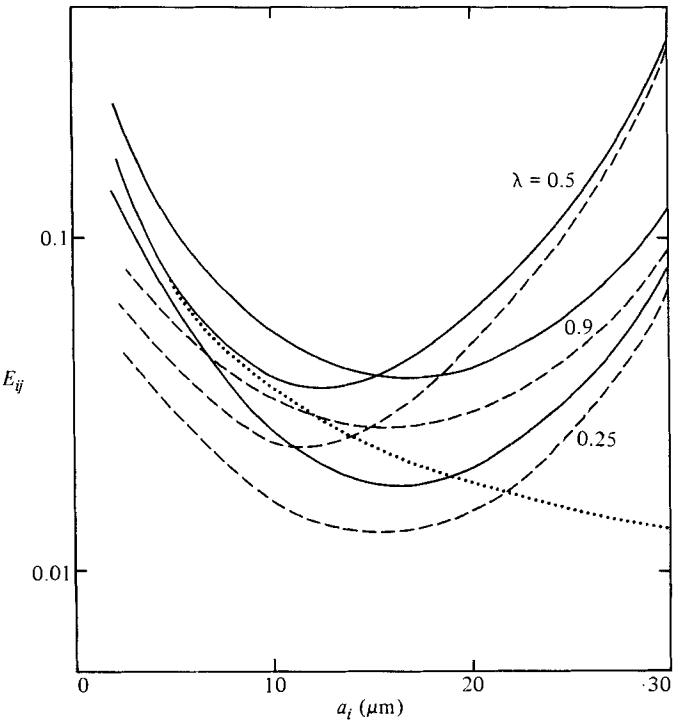

FIGURE 7. The collision efficiency as a function of the radius of the larger sphere for a typical aerosol; $\mu = 1.7 \times 10^{-4}$ P, $\rho = 1.3 \times 10^{-3}$ g cm^{-3}, $\rho_i = \rho_j = 1.0$ g cm^{-3} and $A = 5 \times 10^{-13}$ erg: ——, unretarded van der Waals force; – – – –, retarded van der Waals force; . . . ., computed result for $\lambda = \frac{1}{2}$ when $S = 0$.

(these values are appropriate for water droplets in the atmosphere). In this case, the Stokes number is of order unity when a_i is approximately 10 μm. We thus expect that E_{ij} will decrease with increasing a_i until $a_i \approx 10$ μm, and then will increase as the particle inertia becomes important. This is indeed the case, as can be seen in figure 7, where E_{ij} versus a_i is given for $\lambda = \frac{1}{4}$, $\frac{1}{2}$ and 0.9. Again, the solid lines are from using the unretarded van der Waals potential, and the dashed lines include the retardation effects. For comparison, the dotted line is the collision efficiency for $\lambda = \frac{1}{2}$ under these conditions only with $S = 0$. Evidently, if particle inertia were neglected in aerosol dispersions having $a_i \geqslant 10$ μm, the collision efficiency would then be severely underestimated. The effect of inertia is largest when $\lambda \approx \frac{1}{2}$ because, for $\beta = \gamma = 1$, the dependence of S as a function of λ has a maximum when $\lambda = \frac{3}{7}$. When $\lambda \to 0$ the mass of the smaller particle is negligible, and $S \to 0$; when $\lambda \to 1$ the relative velocity of the two spheres approaches zero, and again $S \to 0$.

5.3. *Comparison of the effects of van der Waals forces and Maxwell slip for aerosol particles*

In the past the influence of van der Waals forces on the collision rate of aerosol particles has been neglected. Instead, the generally accepted mechanism responsible for allowing the particles to overcome the hydrodynamic resistance to contact is the effects of the discrete molecule nature of the surrounding air that become important when the gap between the two spheres is comparable to the main free path λ_m of

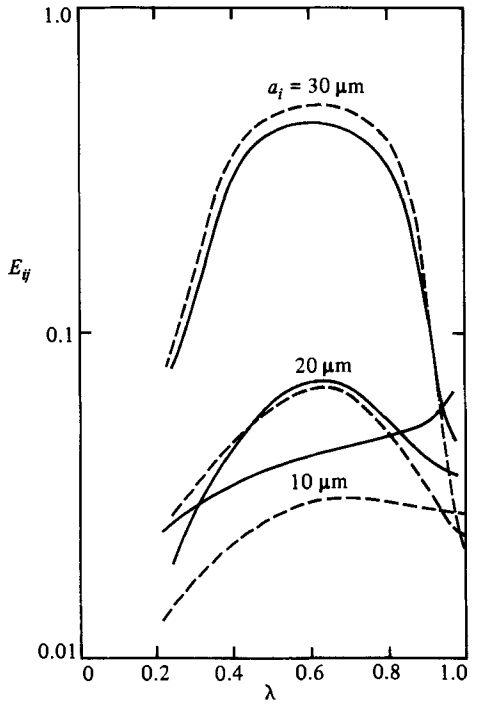

FIGURE 8. The collision efficiency of water droplets in air: ——, unretarded van der Waals force and no slip; – – – –, Maxwell-slip flow model and no interparticle force.

the molecules composing the air ($\lambda_m \approx 0.1$ μm). This has been incorporated in a Maxwell-slip flow model presented by Hocking (1973) and by Davis (1972). In this model, when the gap between the particles is comparable to the mean free path of the air molecules, the boundary condition of no slip at the sphere surfaces is replaced by the condition that the velocity of the air at the surface be proportional to the tangential stress there. The main result is that the force that opposes relative motion along the line of centres is no longer inversely proportional to the gap, but rather it is inversely proportional to the mean free path and only logarithmically dependent on the gap. Thus this gas-kinetic effect allows for collisions between particles to take place, and computations of the collision efficiency of water droplets using this model have been presented by Jonas (1972) and by Davis (1972).

It is instructive to compare these results with the present results and to see the relative importance of Maxwell-slip flow and of van der Waals forces in promoting collisions between sedimenting aerosol particles. This can be made by considering the value of the parameter

$$\epsilon_m = \frac{(6L_1 Q_{ij})^{-\frac{1}{2}}}{2\lambda_m/(a_i + a_j)},$$

which is the ratio of the thickness of the boundary layer where the van der Waals force is important to the mean free path (note that since λ_m is approximately 0.1 μm in the atmosphere, ϵ_m is numerically equal to ϵ_R). When ϵ_m is small the interparticle force becomes important at a value of the gap size for which Maxwell-slip effects are minor; for large ϵ_m the situation is reversed. Moreover, since ϵ_m is proportional to the first power of a_i, we expect that the van der Waals force will be most important for small particles. In figure 8 E_{ij} versus λ is given for $a_i = 10$, 20 and 30 μm using

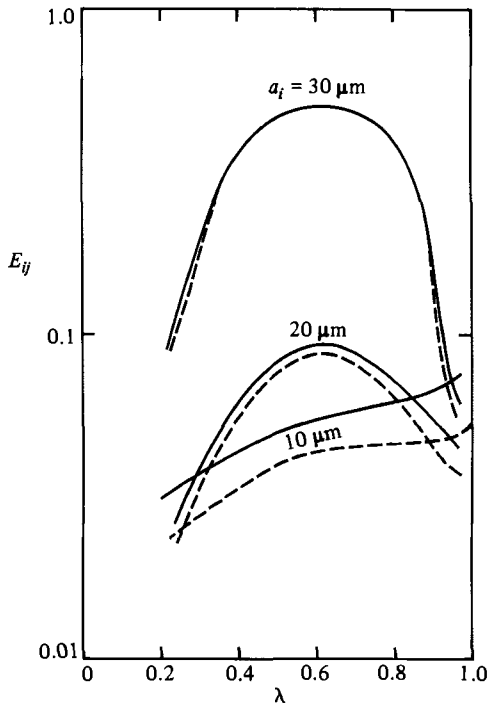

FIGURE 9. The combined effect of van der Waals forces and Maxwell-slip flow on the collision efficiency of water droplets in air: ——, unretarded van der Waals force and Maxwell-slip flow; – – – –, retarded van der Waals force and Maxwell-slip flow.

the same values of the physical parameters as for figure 7. The solid lines are from the present calculation with no slip at the drop surfaces and using (2.2) for the unretarded van der Waals potential. The dashed lines represent the Maxwell-slip flow model with no interparticle force. These latter curves were computed with the present numerical program, only with the force and torque coefficients in (4.1) modified in the same manner as described by Jonas (1972). They agree in all cases to within a few percent of the calculations presented by Jonas. From figure 8 it is apparent that the discrete-molecule effect gives a larger collision efficiency when a_i is greater than 20 μm, but that the interparticle force is the dominant mechanism for particles smaller than this. Thus the van der Waals force has a greater influence in promoting collisions of small drops in clouds than was earlier realized.

Finally, since Maxwell-slip flow and van der Waals forces influence the trajectories of nearly touching spheres over comparable separations, we present in figure 9 the collision efficiency for cloud droplets computed from a trajectory analysis in which both of these effects were included. In general, the collision efficiency is significantly higher than when either effect alone is considered, but its value is less than the sum of the separate contributions given in figure 8. The solid lines in figure 9 are for the unretarded van der Waals potential of (2.2), and the dashed lines are for the retarded potential given by (2.3). Electromagnetic retardation has negligible effect for the larger drops, but it lowers the collision efficiency by as much as 30 % when $a_i = 10$ μm. The dashed lines in figure 9 provide an up-to-date replacement for the collision efficiencies of cloud droplets obtained by Jonas (1972), and can be used in dynamic models for the evolution of the droplet spectrum in a cloud.

This material is based upon work supported by the North Atlantic Treaty Organization under Grant NATO-1982 while the author was a visitor at the Department of Applied Mathematics and Theoretical Physics of the University of Cambridge. Discussions with Professor G. K. Batchelor and Dr E. J. Hinch were instrumental in the development of this work.

REFERENCES

ADLER, P. M. 1981 Heterocoagulation in shear flows. *J. Colloid Interface Sci.* **83**, 106–115.

BATCHELOR, G. K. 1982 Sedimentation in a dilute polydisperse system of interacting spheres. Part 1. General theory. *J. Fluid Mech.* **119**, 379–408.

BATCHELOR, G. K. & WEN, C.-S. 1982 Sedimentation in a dilute polydisperse system of interacting spheres. Part 2. Numerical results. *J. Fluid Mech.* **124**, 495–528.

CURTIS, A. S. G. & HOCKING, L. M. 1970 Collision efficiency of equal spherical particles in a shear flow. *Trans. Faraday Soc.* **66**, 1381.

DAVIS, M. H. 1972 Collision of small cloud droplets: gas kinetic effects. *J. Atmos. Sci.* **29**, 911–915.

HAMAKER, H. C. 1937 The London–van der Waals attraction between spherical particles. *Physica* **4**, 1058.

HOCKING, L. M. 1973 The effect of slip on the motion of a sphere close to a wall and of two adjacent spheres. *J. Engng Maths* **7**, 207–221.

HOCKING, L. M. & JONAS, P. R. 1970 The collision efficiency of small drops. *Q. J. R. Met. Soc.* **96**, 722–729.

JEFFREY, D. J. & ONISHI, Y. 1984 Calculation of the resistance and mobility functions for two unequal rigid spheres in low-Reynolds-number flow. *J. Fluid Mech.* **139**, 261–290.

JONAS, P. R. 1972 The collision efficiency of small drops. *Q. J. R. Met. Soc.* **98**, 681–683.

LIFSHITZ, E. M. 1955 Theory of molecular attraction between solid bodies. *Zh. Eksp. Teor. Fiz.* **29**, 94 (in Russian).

SCHENKEL, J. H. & KITCHENER, J. A. 1960 A test of the Derjaguin–Verwey–Overbeek theory with a colloidal suspension. *Trans. Faraday Soc.* **56**, 161.

SMOLUCHOWSKI, M. VON 1917 Versuch einer mathematischen Theorie der Koagulationskinetik kolloider Lösungen. *Z. Phys. Chem.* **92**, 129.

WACHOLDER, E. & SATHER, N. S. 1974 The hydrodynamic interaction of two unequal spheres moving under gravity through quiescent viscous fluid. *J. Fluid Mech.* **65**, 417–437.

WEN, C.-S. & BATCHELOR, G. K. 1984 The rate of coagulation in a dilute suspension of small particles. *Scientia Sinica* (in press).

ZEICHNER, G. R. & SCHOWALTER, W. R. 1977 Use of trajectory analysis to study stability of colloidal dispersions in flow fields. *AIChE J.* **23**, 243–254.